JOURNAL OF GEOPHYSICAL RESEARCH, VOL. 113, D15S17, doi:10.1029/2007JD008819, 2008

Validation of Tropospheric Emission Spectrometer (TES) nadir ozone profiles using ozonesonde measurements

Ray Nassar,[1] Jennifer A. Logan,[1] Helen M. Worden,[2] Inna A. Megretskaia,[1] Kevin W. Bowman,[3] Gregory B. Osterman,[3] Anne M. Thompson,[4] David W. Tarasick,[5] Shermane Austin,[6] Hans Claude,[7] Manvendra K. Dubey,[8] Wayne K. Hocking,[9] Bryan J. Johnson,[10] Everette Joseph,[11] John Merrill,[12] Gary A. Morris,[13] Mike Newchurch,[14] Samuel J. Oltmans,[10] Françoise Posny,[15] F. J. Schmidlin,[16] Holger Vömel,[17] David N. Whiteman,[18] and Jacquelyn C. Witte[19]

Received 15 April 2007; revised 8 October 2007; accepted 15 November 2007; published 7 May 2008.

[1] We compare Tropospheric Emission Spectrometer (TES) version 2 (V002) nadir ozone profiles with ozonesonde profiles from the Intercontinental Chemical Transport Experiment Ozonesonde Network Study, the World Ozone and Ultraviolet Data Center, the Global Monitoring Division of the Earth System Research Laboratory, and the Southern Hemisphere Additional Ozonesonde archives. Approximately 1600 coincidences spanning 72.5°S–80.3°N from October 2004 to October 2006 are found. The TES averaging kernel and constraint are applied to the ozonesonde data to account for the TES measurement sensitivity and vertical resolution. TES sonde differences are examined in six latitude zones after excluding profiles with thick high clouds. Values for the bias and standard deviation are determined using correlations of mean values of TES ozone and sonde ozone in the upper troposphere (UT) and lower troposphere (LT). The UT biases range from 2.9 to 10.6 ppbv, and the LT biases range from 3.7 to 9.2 ppbv, excluding the Arctic and Antarctic LT where TES sensitivity is low. A similar approach is used to assess seasonal differences in the northern midlatitudes where the density and frequency of sonde measurements are greatest. These results are briefly compared to TES V001 ozone validation work which also used ozonesondes but was carried out prior to improvements in the radiometric calibration and ozone retrieval in V002. Overall, the large number of TES and sonde comparisons indicate a positive bias of approximately 3–10 ppbv for the TES V002 nadir ozone data set and have helped to identify areas of potential improvement for future retrieval versions.

Citation: Nassar, R., et al. (2008), Validation of Tropospheric Emission Spectrometer (TES) nadir ozone profiles using ozonesonde measurements, *J. Geophys. Res.*, *113*, D15S17, doi:10.1029/2007JD008819.

1. Introduction

[2] Tropospheric ozone is difficult to measure from space because the contribution to the measured signal from stratospheric ozone is typically large. The first approach to the determination of tropospheric ozone distributions from satellite measurements involved subtracting the stratospheric ozone column from the total ozone column [*Fishman and*

[1]School of Engineering and Applied Sciences, Harvard University, Cambridge, Massachusetts, USA.
[2]Atmospheric Chemistry Division, National Center for Atmospheric Research, Boulder, Colorado, USA.
[3]Jet Propulsion Laboratory, Pasadena, California, USA.
[4]Department of Meteorology, Pennsylvania State University, University Park, Pennsylvania, USA.
[5]Experimental Studies, Air Quality Research Division, Environment Canada, Downsview, Ontario, Canada.
[6]Medgar Evers College, City University of New York, Brooklyn, New York, USA.
[7]Deutscher Wetterdienst Meteorologisches Observatorium Hohenpeissenberg, Hohenpeissenberg, Germany.
[8]Los Alamos National Laboratory, Los Alamos, New Mexico, USA.
[9]Department of Physics and Astronomy, University of Western Ontario, London, Ontario, Canada.
[10]NOAA Earth System Research Laboratory, Boulder, Colorado, USA.
[11]Physics and Astronomy Department, Howard University, Washington, District of Columbia, USA.
[12]Graduate School of Oceanography, University of Rhode Island, Narragansett, Rhode Island, USA.
[13]Department of Physics and Astronomy, Valparaiso University, Valparaiso, Indiana, USA.
[14]National Space Science and Technology Center, Atmospheric Science Department, University of Alabama in Huntsville, Huntsville, Alabama, USA.
[15]Laboratoire de l'Atmosphère et des Cyclones, CNRS/Université de la Réunion, La Réunion, France.
[16]Laboratory for Hydrospheric Processes, Observational Science Branch, NASA/Wallops Flight Facility, Wallops Island, Virginia, USA.
[17]Cooperative Institute for Research in Environmental Studies, University of Colorado, Boulder, Colorado, USA.
[18]Mesoscale Atmospheric Processes Branch, Goddard Space Flight Center, NASA, Greenbelt, Maryland, USA.
[19]Atmospheric Chemistry and Dynamics Branch, Goddard Space Flight Center, NASA/Science Systems and Applications, Inc., Greenbelt, Maryland, USA.

0148-0227/08/2007JD008819$09.00

Larsen, 1987; *Hudson and Thompson*, 1998; *Ziemke et al.*, 1998, 2005, 2006]. The Global Ozone Monitoring Experiment (GOME) makes nadir measurements of the global distribution of tropospheric ozone columns from space [*Valks et al.*, 2003; *Liu et al.*, 2005, 2006] and a similar Ozone Monitoring Instrument (OMI) tropospheric column retrieval product will soon be available (X. Liu, personal communication, 2006), but these measurements are not capable of providing much information about the vertical distribution of tropospheric ozone. Nadir profiles of tropospheric ozone have been retrieved from measurements by the Interferometric Monitor of Greenhouse gases (IMG) instrument on the ADEOS satellite; however, this limited data set only spans the very brief period of August 1996 to June 1997 [*Coheur et al.*, 2005; *Turquety et al.*, 2002]. Although numerous limb-viewing satellite instruments have the ability to provide good vertical information on ozone in the upper troposphere, they are ineffective in the lower troposphere and their global coverage is typically too sparse to provide reliable global distributions of tropospheric ozone.

[3] The Tropospheric Emission Spectrometer (TES) on the Aura satellite was designed to measure the global vertical distribution of tropospheric ozone, as well as temperature and other important tropospheric species including carbon monoxide, methane and water vapor [*Beer et al.*, 2001; *Beer*, 2006]. Initial validation of TES ozone was carried out by comparing a limited number of early measurements to ozonesondes, using the first version of TES nadir ozone data (V001) [*Worden et al.*, 2007]. In the present work, using version 2 (V002) data, we examine approximately 1600 TES and ozonesonde coincidences spanning 72.5°S–80.3°N from October 2004 to October 2006. As in the initial work, the TES averaging kernel and constraint are applied to the sonde data to account for the TES measurement sensitivity and vertical resolution. With this approach, and a large number of coincidences, we characterize both the bias and variability of the V002 TES nadir ozone data set.

2. TES Measurements and Retrievals

[4] TES is a Fourier transform spectrometer that measures infrared emission of Earth's atmosphere. TES is on the Aura satellite which has a ~705 km sun synchronous polar orbit with an equator crossing time of ~13:45 and a 16 d repeat cycle. Although TES can measure from both the nadir and limb views, nadir is presently the primary scanning geometry used. In cloud-free conditions, the nadir ozone profiles have approximately four degrees of freedom for signal, approximately two of which are in the troposphere, giving an estimated vertical resolution of about 6 km [*Bowman et al.*, 2002, 2006; *Worden et al.*, 2004] with a 5.3 by 8.3 km footprint. The primary measurement mode for TES is the Global Survey (GS), from which the instrument maps the earth in 16 orbits (~26 h). The measurements in a global survey are divided into sequences which take about 82 s each. Prior to May 2005, each of these sequences consisted of three limb scans and two nadir scans. The radiances from the two nadir scans (which were made of the same spot) were averaged together. Nadir measurements in successive sequences were separated by about 544 km, while measurements from the neighboring TES orbit track were separated by 22° longitude. In the present GS configuration, which began on 21 May 2005, a sequence consists of three nadir scans and no limb scans. Each nadir scan within an orbit track in the new GS mode is separated by about 182 km on the ground; therefore, the radiances are not averaged [*Beer*, 2006; *Osterman et al.*, 2006] and the measurements provide more coverage. TES also has special observation modes, the most common one being the Step and Stare (SS), where numerous repetitive measurements are made near a given target, with scans about 6 s apart and separated by 40–45 km along the ground track [*Beer*, 2006; *Osterman et al.*, 2006]. Another common special observation mode is Transect mode, in which repetitive scans are made where the nadir angle changes such that the footprints from subsequent scans are only about 12 km apart. Accumulating transect scans can thus create a nearly contiguous footprint spanning about 500 km.

[5] TES ozone is retrieved from the 9.6 μm ozone absorption band using the 995–1070 cm^{-1} spectral range. The retrievals and error estimation are based on the optimal estimation approach [*Rodgers*, 2000]. TES retrievals are described by *Worden et al.* [2004] and *Bowman et al.* [2002, 2006], with error characterization described by *Kulawik et al.* [2006a]. Temperature, water vapor and ozone are simultaneously retrieved in the first step of the retrieval with other species and parameters retrieved in subsequent steps. Validation of TES temperature retrievals has been carried out by R. Herman et al. (unpublished data, 2007) and validation of TES water vapor is described by *Shephard et al.* [2008a]. The ozone a priori profile (also used as the initial guess) and covariance matrix are derived from a climatology developed using the Model of Ozone and Related Tracers (MOZART) model [*Brasseur et al.*, 1998; *Park et al.*, 2004]. The ozone a priori comes directly from MOZART monthly means which are averaged in 10° latitude by 60° longitude grid boxes. To facilitate use of TES data, the averaging kernel matrix and prior constraint matrix are made available with the data, which may be obtained from the Langley Atmospheric Sciences Data Center (http://eosweb.larc.nasa.gov/PRODOCS/tes/table_tes.html). A detailed description of TES V002 data is given in the TES Level 2 Data User's guide, version 2.0 [*Osterman et al.*, 2006].

3. Ozonesonde Data and Application of the TES Operator

[6] Ozonesondes make in situ measurements of temperature, pressure, humidity and ozone from balloons launched from stations around the world. The sondes provide profiles with a vertical resolution of about 150 m, up to a maximum altitude of about 35 km, although not all measurements reach this height. We use ozonesonde measurements from: the Intercontinental Chemical Transport Experiment Ozonesonde Network Study (IONS) [*Thompson et al.*, 2007b, 2007c] campaign in 2006 (IONS-06) (http://croc.gsfc.nasa.gov/intexb/ions06.html), the World Ozone and Ultraviolet Data Center (WOUDC) (http://www.woudc.org), the Global Monitoring Division (GMD) of the Earth System Research Laboratory (http://www.esrl.noaa.gov/gmd) and the Southern Hemisphere Additional Ozonesonde (SHADOZ) archive (http://croc.gsfc.nasa.gov/shadoz) [*Thompson et al.*, 2003a, 2003b, 2007a].

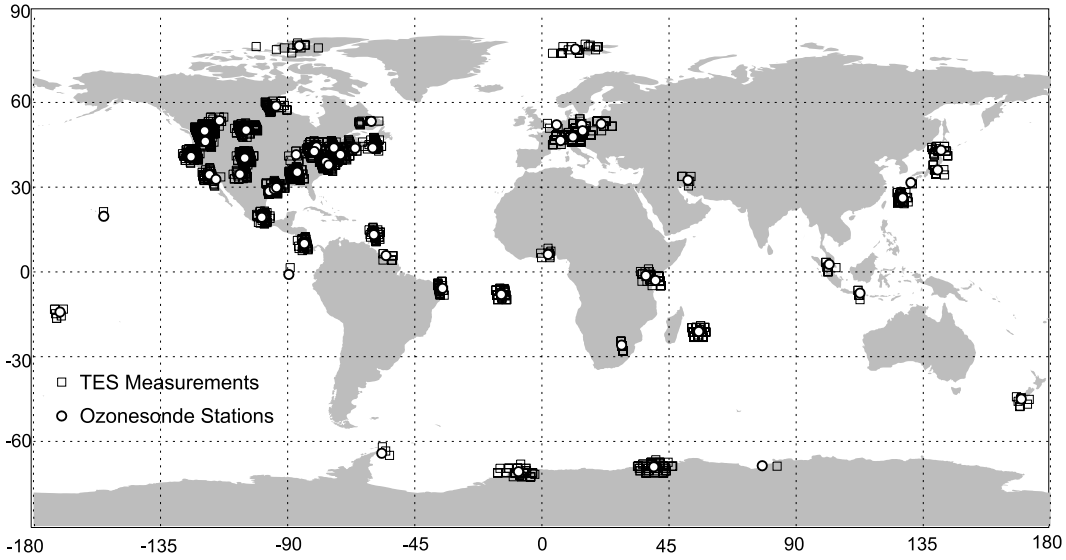

Figure 1. Map of approximately 1600 TES and ozonesonde coincidences.

[7] The accuracy of ozone measured from sondes is often quoted as about ± 5% [*Stratospheric Processes and their Role in Climate, International Ozone Commision, and Global Atmosphere Watch*, 1998], but actually depends on numerous factors. A variety of types of ozonesondes exist, but the most common type used in this work is the electrochemical concentration cell (ECC) sonde which relies on the oxidation reaction of ozone with a potassium iodide (KI) solution [*Komhyr et al.*, 1995]. (The main exceptions being the Hohenpeissenberg station which uses Brewer-Mast (BM) sondes and the four stations in Japan which use KC type sondes.) ECC sondes are made by two different manufacturers and can operate with a range of KI solution strengths, buffer types and preparation procedures. Sonde performance was evaluated in a series of experiments [*Smit et al.*, 2007], but the study was based on a small number of sonde measurements. Their work indicates a precision of better than ±(3–5)% and an accuracy of about ±(5–10)% up to 30 km altitude if standard operating procedures for ECC sondes are used, and suggests a median high bias of about 5% for ECC sondes relative to an ultraviolet (UV) photometer.

[8] Overhead columns are measured independently by a Dobson or Brewer instrument for some sonde profiles. If an overhead column measurement is available, as for most WOUDC data, a correction factor (CF) is calculated, which can also be used to screen the data. For the SHADOZ data set, no overhead measurements are available, but the data were screened by integrating the profiles and comparing to ozone columns from the Total Ozone Mapping Spectrometer (TOMS). A more detailed description of the screening approach is given by *Worden et al.* [2007]. No systematic screening was applied to the IONS-06 data, but a very small number of obviously erroneous profiles were rejected.

[9] For sonde measurements that did not reach 10 hPa, we approximated the unmeasured part of the stratosphere by appending the TES a priori profile. Since the original sonde data are provided on various irregular pressure grids, all data are interpolated to a fine level pressure grid (800 levels from 1260 hPa to 0.46 hPa), then a mapping matrix is used to interpolate to the 67 pressure level TES grid (from 1212 to 0.1 hPa). The TES averaging kernel $\mathbf{A}_{\mathrm{TES}}$ and a priori constraint vector $\mathbf{x}_{\mathrm{prior}}$ are together referred to as the TES operator. Applying the TES operator to the sonde data $\mathbf{x}_{\mathrm{sonde}}$ (which is now on the TES pressure grid) yields $\mathbf{x}_{\mathrm{sondeTESop}}$, a profile which accounts for the TES sensitivity and vertical resolution

$$\mathbf{x}_{\mathrm{sondeTESop}} = \mathbf{x}_{\mathrm{prior}} + \mathbf{A}_{\mathrm{TES}}\left[\mathbf{x}_{\mathrm{sonde}} - \mathbf{x}_{\mathrm{prior}}\right]. \quad (1)$$

[10] To state this in another way, $\mathbf{x}_{\mathrm{sondeTESop}}$ is the profile that would be retrieved from TES measurements for the same air sampled by the sonde in the absence of other errors. It is important to note that with this approach, the TES-sonde difference ($\mathbf{x}_{\mathrm{TES}} - \mathbf{x}_{\mathrm{sondeTESop}}$) is not biased by the TES a priori. Our approach is based on *Rodgers and Connor* [2003] and the application to TES data is described in more detail by *Worden et al.* [2007] along with figures depicting the TES ozone averaging kernels under clear sky and cloudy conditions. For the remainder of the paper, any comparisons between TES and ozonesonde data have had the TES operator applied.

4. Coincidence Criteria and TES Data Screening

[11] A review of the literature on validation of atmospheric measurements from satellites, reveals the application of a range of coincidence criteria. In the first validation of TES ozone [*Worden et al.*, 2007], only a limited number of TES and sonde coincidences were available, therefore to obtain enough comparisons, a time separation of ±48 h and a 600 km radius from the sonde station were used as the coincidence criteria. In this work, we have applied criteria of ±9 h and a 300 km radius, which was partly based on a separate analysis comparing coincidence criteria using measurements from the SAUNA (Sodankylä Total Column Ozone Intercomparison) ozonesonde campaign from Sodankylä, Finland (67.4°N, 26.6°E) between 27 March

Table 1. Ozonesonde Station Locations, Data Providers, and the Number of TES Coincidences

Ozonesonde Station	Latitude	Longitude	Data Source	N[a]
Eureka	80.0	−85.9	WOUDC	11
Ny Ålesund	78.9	11.9	WOUDC	20
Churchill	58.7	−94.1	WOUDC	28
Edmonton	53.6	−114.1	WOUDC	13
Goose Bay	53.3	−60.4	WOUDC	8
Legionowa	52.4	21.0	WOUDC	16
Lindenberg	52.2	14.1	WOUDC	11
De Bilt	52.1	5.2	WOUDC	3
Bratt's Lake	50.2	−104.7	IONS/WOUDC	56
Praha	50.0	14.4	WOUDC	17
Kelowna	49.9	−119.4	IONS/WOUDC	117
Hohenpeissenberg	47.8	11.0	WOUDC	97
Payerne	46.5	6.6	WOUDC	20
Richland	46.2	−119.2	IONS	35
Egbert	44.2	−79.8	IONS/WOUDC	24
Sable Island	44.0	−59.9	IONS	26
Yarmouth	43.9	−66.1	IONS/WOUDC	18
Paradox	43.9	−73.6	IONS	35
Sapporo	43.1	141.3	WOUDC	16
Walsingham	42.6	−80.6	IONS	27
Narragansett	41.5	−71.3	IONS	48
Valparaiso	41.5	−87.0	IONS	7
Trinidad Head	40.8	−124.2	IONS/WOUDC/GMD	83
Boulder	40.3	−105.2	IONS/WOUDC/GMD	86
Beltsville	39.0	−76.5	IONS	22
Wallops Island	37.9	−75.5	IONS/WOUDC	64
Tateno	36.1	140.1	WOUDC	11
Huntsville	35.3	−86.6	IONS/WOUDC	77
Socorro	34.6	−106.9	IONS	24
Table Mountain	34.4	−117.7	IONS	32
Holtville	32.8	−115.4	IONS	7
Isfahan	32.5	51.7	WOUDC	5
Kagoshima	31.6	130.6	WOUDC	1
Houston	29.7	−95.3	IONS/WOUDC	52
Ron Brown[b]	28.1 to 29.9[b]	−93.9 to −96.5[b]	IONS	20
Naha	26.2	127.7	WOUDC	35
Hilo	19.7	−155.1	WOUDC/GMD	1
Mexico City	19.4	−98.6	WOUDC	16
Tecamec	19.3	−99.2	IONS	14
Barbados	13.2	−59.5	IONS/GMD	33
Heredia	10.0	−84.1	SHADOZ/GMD	43
Cotonou	6.2	2.2	SHADOZ	8
Paramaribo	5.8	−55.2	SHADOZ	9
Kuala Lampur	2.7	101.7	SHADOZ	8
San Cristobal	−0.9	−89.6	SHADOZ/GMD	1
Nairobi	−1.3	36.8	SHADOZ	19
Malindi	−3.0	40.2	SHADOZ	23
Natal	−5.8	−35.2	SHADOZ	31
Java	−7.5	112.6	SHADOZ	5
Ascension Island	−8.0	−14.4	SHADOZ	53
American Samoa	−14.2	−170.6	SHADOZ/GMD	7
Reunion Island	−21.1	55.5	SHADOZ	58
Pretoria	−25.9	28.2	SHADOZ	16
Lauder	−45.0	169.7	WOUDC	9
Marambio	−64.2	−56.7	WOUDC	3
Davis	−68.6	78.0	WOUDC	1
Syowa	−69.0	39.6	WOUDC	60
Neumayer	−70.7	−8.3	WOUDC	44
TOTAL				**1634**

[a] N refers to the number of coincidences with this station in the present analysis although more coincidences may be available. Soundings coincident with multiple TES measurements are counted multiple times, as are the 44 TES measurements coincident with sonde profiles from two stations.

[b] Ron Brown is a ship which serves as a mobile sonde station and was situated in the Gulf of Mexico for the IONS-06 campaign.

to 14 April 2006. Although those comparisons were Transect observations (which involve larger viewing angles than GS or SS observations), they indicated that over a reasonable range, the choice of coincidence criteria affects the variability determined from the comparisons much more than the bias determination. Ultimately, our criteria were selected to balance the fact that the probability of measuring an air parcel with different characteristics increases with the distance and time separation, along with the need to have a sufficient number of profiles available for a good statistical treatment. It should also be noted that over the course of a measurement, an ozonesonde undergoes horizontal drift; therefore, the exact separation between the TES and sonde measurements may differ from the stated distances which are based on the position of the sonde station.

[12] We found 1634 TES and ozonesonde coincidences from October 2004 to October 2006. The frequency of coincidences was highest in 2006 because of the increase in frequency of TES measurements in May 2005 and the large number of sonde launches, especially during the IONS-06 campaign. Figure 1 shows a map of ozonesonde stations and their coincident TES measurements, with details given in Table 1. Of the 1634 coincidences, 44 TES profiles were simultaneously coincident with sonde profiles from two stations, in which case the profiles from the two stations were averaged, resulting in 1590 unique pairs for validation. The coincidence pairs were divided into six latitude zones on the basis of the latitude of the sonde station (see Table 2) to group regions with similar ozone profiles. The northern midlatitudes, northern subtropics and tropics have more coincidences than other zones as a result of the high number of sonde stations located in these areas, as well as the high frequency of measurements during IONS-06.

[13] TES measurements were screened using the "TES ozone data quality flag" [*Osterman et al.*, 2006] and the "emission layer flag." The case study which resulted in development of the emission layer flag is described in section 6. Although these error flags do not identify all erroneous retrievals, suspicious unflagged profiles (∼1–2% of all pairs depending on the criteria used), which appear as large outliers in Figure 2, have not been removed to minimize subjectivity in the comparisons.

[14] Since cloud top pressure and cloud effective optical depth are jointly retrieved from TES measurements [*Kulawik et al.*, 2006b; *Eldering et al.*, 2008] along with trace gas species, they can be used to aid in screening the TES data. Profiles with thick high clouds in the field of view were removed because these obscure the infrared emission from the lower troposphere, greatly reducing TES sensitivity. The number of profiles in each zone excluded because of clouds is given in Table 2. Profiles with a cloud top pressure less than 750 hPa (cloud top height above ∼2.5 km) with an effective optical depth greater than 2.0 are considered to be obscured by clouds. The optical depth threshold was selected by inspection of the averaging kernels. It permits some cloudiness and thus some reduction in the averaging kernel, but it is a slightly stricter cloud criterion than an effective optical depth >3.0 used by *Worden et al.* [2007]. Inclusion of cloudy profiles would artificially make the TES and sonde agreement better in the lower troposphere because for cloudy scenes the ozone averaging kernel approaches zero, causing the retrieval to revert back to the a priori. Since the TES

Table 2. Latitude Zones, the Number of Coincident Pairs Used, and the Number Rejected Based on Clouds and the TES Error Flags

Latitude Zone	Nominal Latitude Range	Latitude Range of TES Measurements	*N* Included	*N* Cloudy	*N* Flagged
Arctic[a]	56–90°N	56.6–80.3°N	35	8	16
Northern midlatitudes	35–56°N	35.0–54.8°N	699	174	31[b]
Northern subtropics	15–35°N	15.0–35.0°N	169	23	5[b]
Tropics	15°S–15°N	15.0°S–15.0°N	203	12	24[b]
Southern low and midlatitudes	15–60°S	15.0–47.7°S	56	10	17
Antarctic	60–90°S	61.9–72.5°S	67	9	32

[a]Churchill (58.7°N, 94.1°W) coincidences which are in the Subarctic were grouped with the Arctic in order to improve statistics in this zone.
[b]Flagged TES measurements coincident with IONS and IONS-06 soundings were not compared and thus not counted in this tally.

averaging kernel is also applied to the sonde profile, the residual from subtracting the two quantities is then nearly zero.

5. TES/Ozonesonde Comparisons

[15] Ozone difference profiles are shown in Figure 2 for TES minus sonde. The southern subtropics and midlatitudes were combined as a single zone because of the small number of measurements. Percent differences are shown up to 10 hPa (left), while the absolute difference profiles are only shown up to 200–300 hPa to focus on the troposphere (right). All individual profiles are plotted in gray with black lines overlaid to indicate the mean and one standard deviation range.

[16] In all six latitude zones, there is an overall positive bias in the TES measurements relative to the sondes. The mean difference or bias is generally in the 0–15% range for the troposphere. The absolute value of the bias and standard deviation generally increase near the tropopause and in the lower stratosphere, but this translates to a small percent difference as ozone levels are higher there. In the tropics and subtropics the bias exceeds 20% at low altitudes. In these latitude zones as well as the northern midlatitudes, both the mean and standard deviation at low altitudes are inflated by a few large outliers that have been left in the comparison. The outliers only represent about 1–2% of all unflagged profiles in these latitude zones. It has been determined that these anomalous profiles occur over both land and ocean, and do not appear to be related to the absolute level of ozone. Nearly no low altitude bias is seen in the Arctic and Antarctic where ozone levels are low and the brightness temperature at the surface is very low, resulting in low sensitivity, and thus causing the TES retrieval to revert back to the a priori. The region from about 70–300 hPa in the southern low and midlatitudes is the only real exception to the general positive bias. These low TES measurements mainly originate from coincidences with sondes from the subtropical stations at Reunion Island and Pretoria. The low bias did not appear to relate to season, or any obvious characteristic that would distinguish these coincidences from the rest.

[17] The profile comparisons in Figure 2 give a good overview of the variability and bias in TES profiles, but since there are approximately 2 degrees of freedom for signal in the troposphere, a proper quantitative analysis should account for this. In Figure 3, TES versus sonde correlations are shown for the lower troposphere (LT) defined as the surface to 500 hPa and the upper troposphere (UT) defined as 500 hPa to the tropopause pressure determined as the pressure at the TES temperature minimum or a given cutoff pressure (which ever is larger). The cutoff pressure for each latitude zone was 300 hPa for Arctic, Antarctic and northern midlatitudes and 200 hPa elsewhere. The error bars in Figure 3 show the mean of the TES errors, since there is a correlation between the levels used for determination of the mean. The bias of the mean, the standard deviation or root-mean-square error (RMS) and the correlation coefficient (R) are also given in Figure 3.

[18] The mean UT biases range from 2.9 ppbv in the tropics to 10.6 ppbv in the Antarctic, while the LT biases range from 0.7 ppbv in the Antarctic to 9.2 ppbv in the tropics. The bias generally has a positive additive (shift) component and a negative multiplicative (slope) component. In the northern midlatitudes where the most coincidences were available, the correlation is mainly compact, but a few high outliers have decreased the R value and increased the bias and standard deviation. In the northern subtropics and tropics, the correlation is excellent in the UT but poor in the LT as a result of a few outliers. The low bias in the southern low and midlatitude profiles between 70 and 300 hPa does not show up in the correlations since it is predominantly above the tropopause. The apparently good correlations seen in the Antarctic and Arctic LT result from the fact that the retrieval has very low sensitivity there and is reverting back to the a priori as mentioned earlier. These Arctic and Antarctic correlations should not be interpreted as implying that TES measurement capability is good in these regions, but they provide an example of the influence that would have occurred if cloudy coincidences (also with low measurement sensitivity) had been included in our statistics for other latitude zones.

[19] There were a sufficient number of coincidences in the northern midlatitudes to permit the investigation of seasonal variability. Difference profiles for the four seasons are shown in Figure 4 and the corresponding correlations in Figure 5. The altitude of the peak in the mean percent difference profiles was lowest in the winter and highest in the summer, which likely relates to the changing tropopause height and variability of ozone [*Logan*, 1999]. The seasonal division also shows that the low altitude outliers predominantly occur in the summer and to a lesser degree in the spring, and that the summer northern midlatitude bias profiles somewhat resemble the northern subtropics or the tropics in the upper troposphere.

[20] The northern midlatitude winter UT correlations have the largest bias (17.5 ppbv) and RMS (25.6 ppbv) of all seasons. The large RMS is likely attributable to the high variability in upper tropospheric and lower stratospheric ozone [*Logan*, 1999], but may also relate to the low tropopause heights in the northern midlatitude winter which reduces the degrees of freedom for signal in the troposphere.

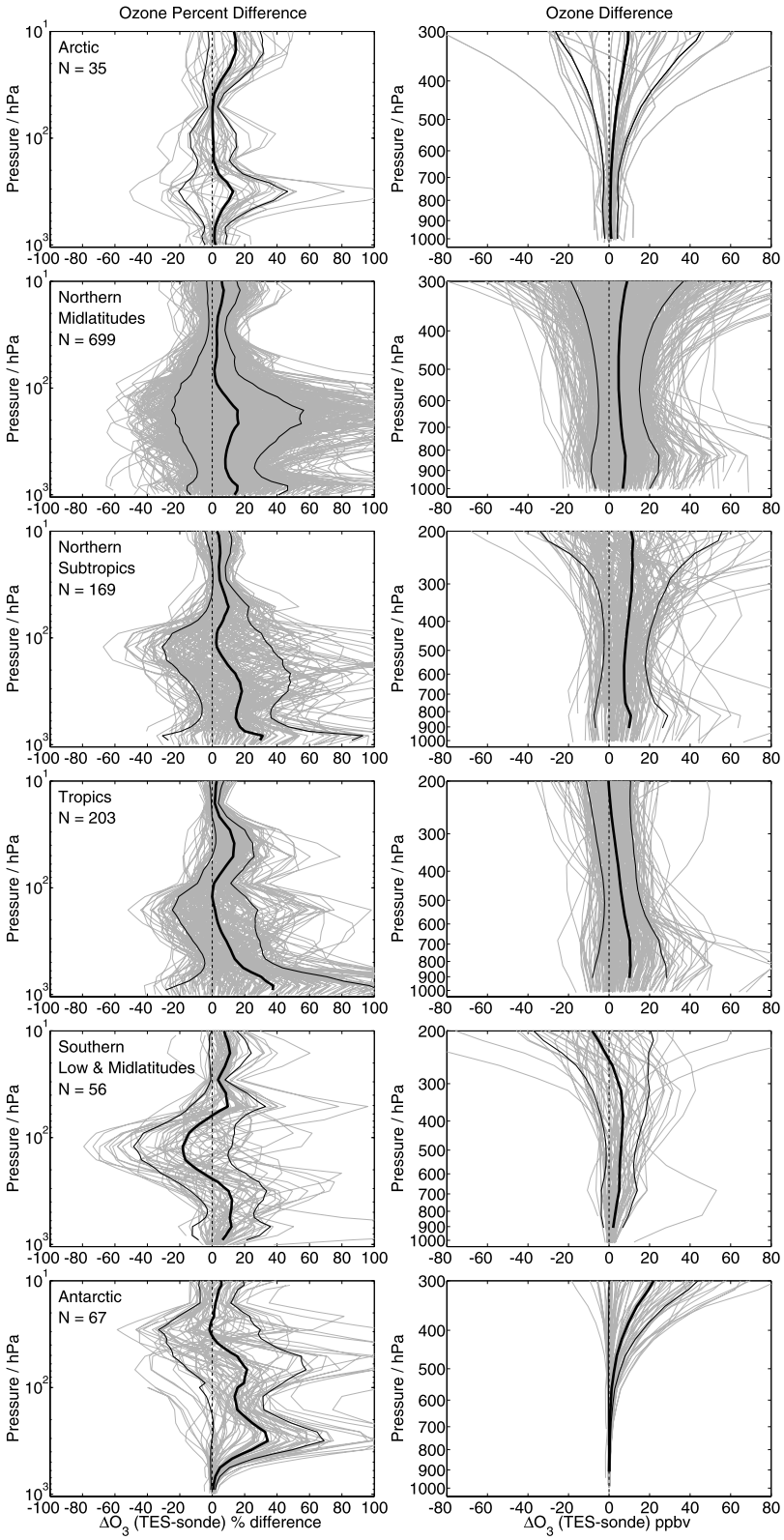

Figure 2. TES-sonde ozone percent differences and absolute differences in six latitude zones. Individual profiles are shown in gray, and the mean and 1 standard deviation range are overlaid in black. *N* is the number of profiles plotted after removing cloudy scenes and flagged TES data.

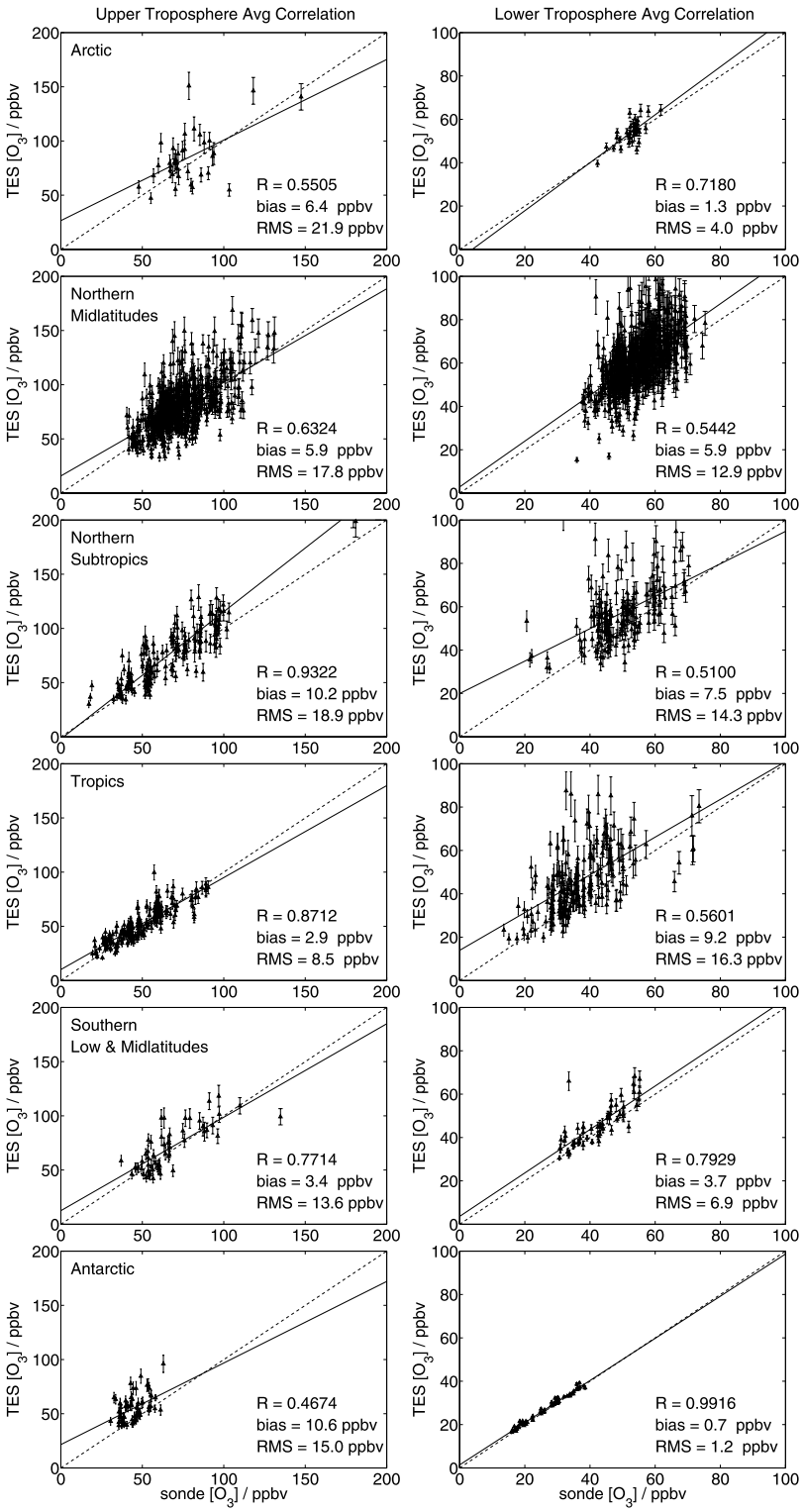

Figure 3. TES versus sonde UT and LT mean correlations. The solid line is the linear fit, and the dotted line shows a 1:1 relationship for reference. The bias and RMS in ppbv and the correlation coefficient are given in the lower right corner of each plot. Arctic and Antarctic LT plots only show tight correlations because these regions suffer from low TES sensitivity. *N* for each zone is given in Figure 2.

The winter and spring UT correlations have the largest biases but also have the highest correlation coefficients. Although a low positive bias was determined for the summer UT, it is accompanied by a relatively large RMS and a low correlation coefficient. In the LT, the bias is fairly constant at 5.2–6.5 ppbv accompanied by an RMS of 10.0–14.3 ppbv, with the exception of the fall where both the bias

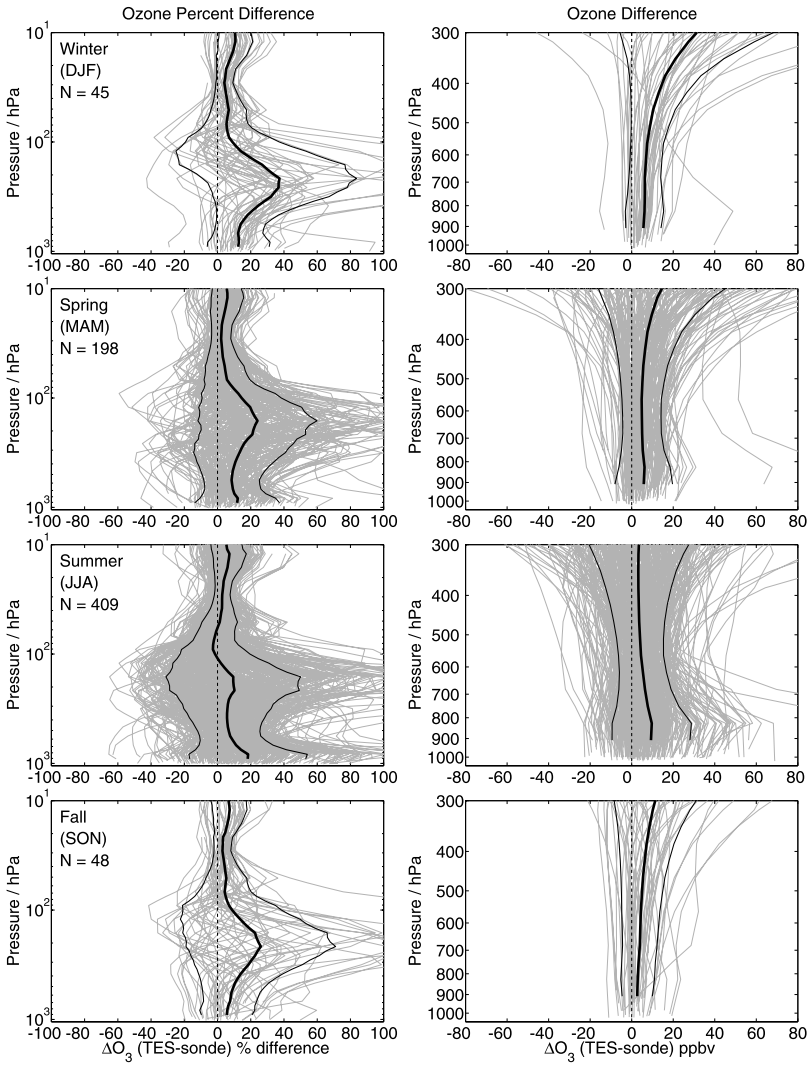

Figure 4. TES-sonde ozone percent differences and absolute differences for the four seasons (months abbreviated in parentheses) in the northern midlatitudes (35–56°N). Individual profiles are shown in gray, and the mean and 1 standard deviation range are overlaid in black. *N* is the number of profiles plotted after removing cloudy scenes and flagged TES data.

and RMS are slightly lower. The LT correlation coefficients are fairly constant ranging from 0.47 to 0.57.

[21] Atmospheric variability with respect to ozone was investigated further by examining the difference between pairs of ozonesonde profiles which came close to meeting the TES/sonde coincidence criteria, as shown in Table 3 and Figure 6. The largest separation in these 10 pairs is 349 km and 8.89 h. Only sonde pairs with one or more coincident TES measurements were used to allow for application of the TES operator. When multiple TES measurements were coincident with the pair, the mean of the available TES operators was applied. Although procedural differences between sonde measurements and the use of different sonde types (for example Hohenpeissenberg BM sondes and Praha ECC sondes [*DeBacker et al.*, 1998]) may account for some of the difference between the two sonde profiles, the majority of the difference can be attributed to atmospheric variability. Figure 6 shows that the variability of the profile pairs is significant, with the mean variability peaking at about 20% near the tropopause. It is evident that the shape and range of the sonde difference profiles in Figure 6 are similar to those of the TES-sonde differences in Figures 2 and 4. This strongly suggests that atmospheric variability likely accounts for a significant portion of variability in the TES-sonde differences as well, thus reducing the potential contribution from the errors in the TES measurements. Furthermore, this example may underestimate true ozone variability because none of the sonde profile pairs were in the winter when the greatest northern midlatitude variability is expected on the basis of the RMS in our seasonal comparisons and on previous work [*Logan*, 1999].

6. Emission Layer Flag

[22] In addition to the standard TES data quality flag, a second flag was developed in a case study that compared TES transect measurements to sonde measurements during the winter at the Southern Great Plains Atmospheric Radiation Measurement (ARM-SGP) facility (36.6°N, 97.5°W).

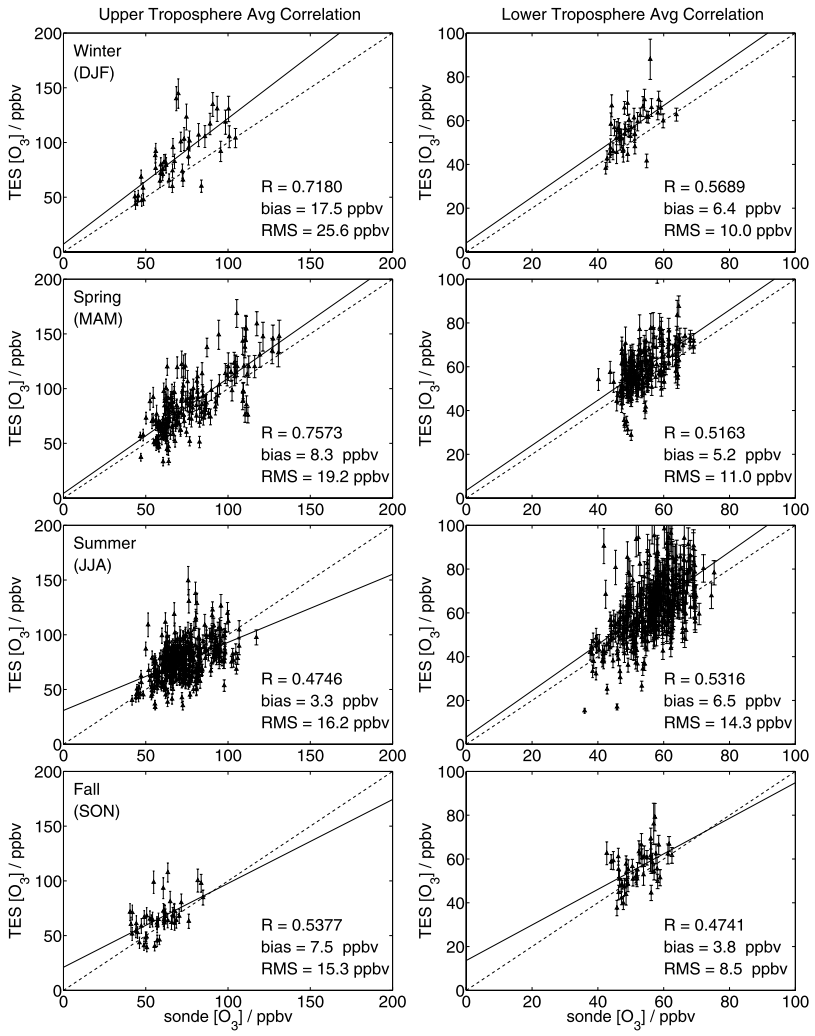

Figure 5. TES versus sonde UT and LT mean correlations for the four seasons (months abbreviated in parentheses) in the northern midlatitudes (35–56°N). The solid line is the linear fit, and the dotted line shows a 1:1 relationship for reference. The bias and RMS in ppbv and correlation coefficient are given in the lower right corner of each plot. *N* for each season is given in Figure 4.

The sondes were launched by F. Schmidlin (NASA Wallops), from 18 January to 16 February 2006, for both night and day Aura overpasses at the ARM-SGP site and were made within 250 km and less than 1 h from the TES observations. Figure 7 shows comparisons with the ARM-SGP ozonesonde measurements (5 night and 4 d transect runs). These comparisons have been critical in identifying erroneous TES retrievals that can sometimes result when the lowest layers of the atmosphere are in emission (i.e., warmer than the surface). Increased sensitivity in the lowest layers due to higher thermal contrast can lead to an overestimate of ozone abundance near the surface while still producing a minimum in the radiance residuals since the ozone in emission would tend to radiatively cancel the ozone in absorption in the layers above. Constraints in the current retrieval algorithm do not prevent this but the condition is now identified with the "emission layer flag," which flags profiles when the thermal contrast ($T_{atmosphere} - T_{surface}$) over the lowest three layers in the TES retrieval is greater than 1 K and the ozone in these layers is greater than the initial guess by more than 15 ppbv. Figure 7 demonstrates the effect of the emission layer flag on night observations, compared to day observations, which did not have emission layer conditions. Since the measurements in this case study were transect measurements often with higher viewing angles (with the respect to the zenith) than SS or GS measurements, these additional 283 profiles have not been included in the bulk northern midlatitude statistics

Table 3. Ozonesonde Pairs Which Approximately Meet the TES/Sonde Coincidence Criteria

Measurement Date	Ozonesonde Station Pair	Δt/hr	Δd/km
30 March 2005	Lindenberg-Praha	0.73	246
4 April 2005	Hohenpeissenberg-Praha	3.89	349
6 March 2006	Hohenpeissenberg-Praha	8.89	349
7 April 2006	Hohenpeissenberg-Praha	4.89	349
7 August 2006	Narragansett-Paradox	1.30	329
16 August 2006	Narragansett-Paradox	0.82	329
21 August 2006	Houston-Ron Brown	0.60	90.2
23 August 2006	Narragansett-Paradox	0.50	329
23 August 2006	Houston-Ron Brown	1.10	234
28 August 2006	Beltsville-Wallops	0.60	160

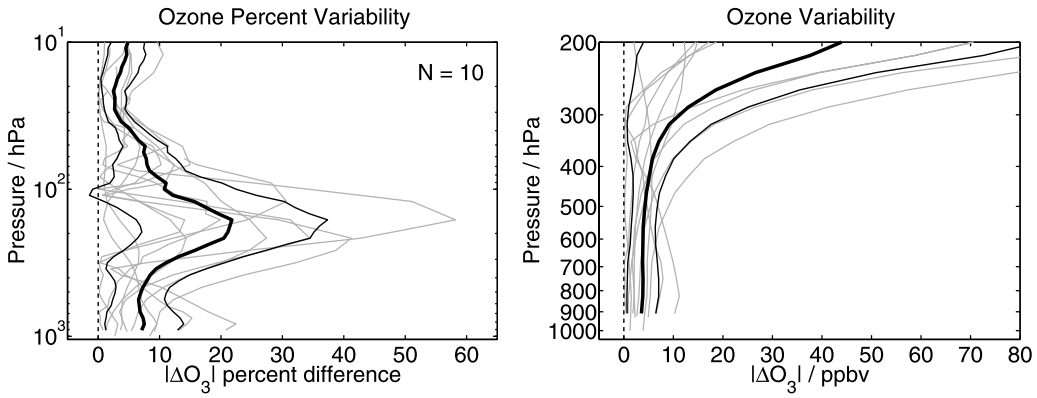

Figure 6. Ozone variability based on pairs of ozonesonde measurements that approximately meet the TES/sonde coincidence criteria. The coincident sonde pairs ranging from 28.1°N to 52.2°N are given in Table 3. The TES-averaging kernels and constraints have been applied before determining differences between the two sonde measurements. The mean and standard variability of a single profile are overlaid in black with the number of pairs given as *N*.

for which a large number of coincidences were already available.

7. Discussion

[23] In the present work, the TES operator has been applied to ozonesonde profiles. This facilitates direct comparison by smoothing the sonde data with the TES averaging kernel and also allows calculation of a TES-sonde difference that is not biased by the TES a priori. While this approach has advantages, one must also be careful not to mistake a lack of sensitivity or low $\mathbf{A}_{\mathrm{TES}}$ (as in the case of cloudy scenes or Arctic/Antarctic conditions in the LT) for good agreement between the data sets (low $\mathbf{x}_{\mathrm{TES}} - \mathbf{x}_{\mathrm{sondeTESop}}$). We have accounted for this in the Arctic and Antarctic by identifying the low sensitivity by inspection of the averaging kernels, and in the case of cloudy scenes using the effective optical depth in the LT to screen out such cases.

[24] The present study provides the largest and widest ranging evaluation of TES ozone measurements to date. Our comparisons indicate a positive bias with values of 2.9–10.6 ppbv for the UT, and 3.7–9.2 ppbv for the LT, depending on latitude zone (see Table 4). These tropospheric biases agree with evaluation of TES ozone using airborne differential absorption LIDAR [*Richards et al.*, 2008]. We emphasize however, that the exact value of the bias has little meaning as the RMS is much larger than the bias in all regions. This was confirmed by taking random samples of about 70 coincidences in the northern midlatitudes and recalculating both quantities ten times. The test yielded biases of 2.9–9.3 ppbv for the UT and 3.1–8.2 ppbv for the LT, with RMS values (which indicate the variability on a single profile) ranging from 10.1 to 20.5 ppbv. Therefore, although we can surely confirm a statistically significant overall positive bias of a few ppbv, it cannot be narrowed much beyond the 3–10 ppbv range. Using the standard error of the mean (where $\sigma_{\mathrm{mean}} = \sigma/\sqrt{N}$) is one potential approach, whereby the biases can sometimes be distinguished from one another at the 2σ confidence level, but this probably overestimates the certainty of the biases. For the UT, the tropics and the southern low and midlatitudes are likely at the lower end of the 3–10 ppbv range, the

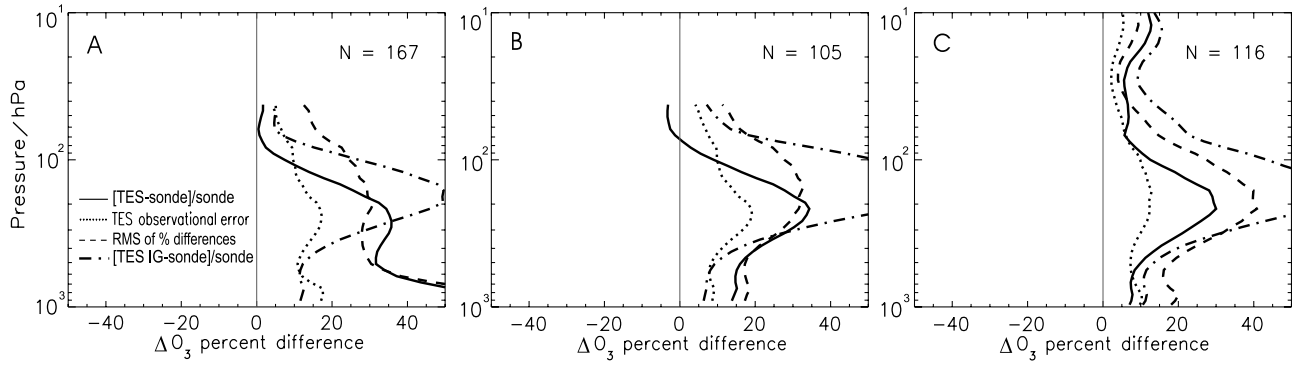

Figure 7. TES-sonde ozone percent differences for the ARM-SGP transect case study. The maximum altitude is determined by the lowest sonde height in the ensemble. (a) The average TES-sonde percent difference and RMS for night observations, screened only by the general data quality flag. Note the large values for both average difference and RMS near the surface. (b) Night observations excluding TES scenes with an emission layer identified. (c) Day observations which did not have any emission layer scenes detected. IG indicates initial guess.

Table 4. UT and LT Biases, Standard Deviations (σ), and the Standard Errors of the Mean ($\sigma_{mean} = \sigma/\sqrt{N}$) in Six Latitude Zones

Latitude Zone	Latitude Range of TES Measurements	UT Bias ± σ, ± σ_{mean} (ppbv)	LT Bias ± σ, ± σ_{mean} (ppbv)
Arctic	56.6–80.3°N	6.4 ± 21.9, ± 3.7	n/a[a]
Northern midlatitudes	35.0–54.8°N	5.9 ± 17.8, ± 0.7	5.9 ± 12.9, ± 0.5
Northern subtropics	15.0–35.0°N	10.2 ± 18.9, ± 1.5	7.5 ± 14.3, ± 1.1
Tropics	15.0°S–15.0°N	2.9 ± 8.5, ± 0.6	9.2 ± 16.3, ± 1.1
Southern low and midlatitudes	15.0 –47.7°S	3.4 ± 13.6, ± 1.8	3.7 ± 6.9, ± 0.9
Antarctic	61.9–72.5°S	10.6 ± 15.0, ± 1.8	n/a[a]

[a]The bias, standard deviation, and standard errors of the mean determined in these regions were not valid because the TES measurement sensitivity was low.

northern midlatitudes and Arctic likely in the middle, and the northern subtropics and Antarctic are at the high end of the range. In the LT, Arctic and Antarctic biases are inconclusive since the sensitivity is so low, but the southern low and midlatitudes are likely at the low end of the range, while the remaining zones are likely somewhat higher.

[25] Since the probability of mismatching profile pairs is expected to increase with distance and time separation, our coincidence criteria (±9 h and a 300 km radius from the sonde station) were selected to balance this fact with the need to have a sufficient number of profiles available for a good statistical treatment. Figure 6 and the related analysis indicate that some contribution to the variability can clearly be attributed to TES and sonde profiles mismatched in space and time, i.e., each measuring air containing different levels of ozone. The effect (if any) that atmospheric variability has on the bias is difficult to asses and quantify. Since the northern midlatitudes had the most profiles available, we tested the effect of tightening the coincidence criteria to ±3 h and 100 km, which resulted in 67 profiles. The tighter coincidence criteria yield biases for the UT and LT that are slightly smaller than those with the standard criteria but the difference is not statistically significant if the standard deviation is considered (see Table 5). The values for the standard error of the mean are also given in Table 5. Using σ_{mean} provides further confirmation that any reduction in the bias as a result of tightening the coincidence criteria is not statistically significant and also indicates that tightening the coincidence criteria reduces the standard deviation variability at a statistically significant level for the both the LT and UT, since the difference in the standard deviation variability (Table 5) for the two sets of coincidence criteria is greater than the combined standard errors from the two means. Therefore, if we had carried out the work with tighter coincidence criteria throughout, the value of the bias would not be statistically different, but the standard deviation would be less. This result is in agreement with previous work involving comparisons to SAUNA data (described earlier) and is perhaps predictable since in theory, the random mismatching of profiles should only add random error but should not introduce a positive or negative bias.

[26] With the TES tropospheric ozone bias mainly less than 15%, and the accuracy of ozonesonde profiles estimated to be 5–10% with a potential bias of 5% (relative to a UV photometer) [*Smit et al.*, 2007], the error contribution by ozonesonde measurements should perhaps not be so easily dismissed. However, the fact that a positive bias of less than 15% was also determined by *Richards et al.* [2008] who compared to a completely different measurement technique and used a different set of coincidence criteria, strongly supports the idea that the bias is unrelated to atmospheric variability, and that the contribution to the bias from sondes is not very large. Issues such as biases between different types of ozonesondes, or biases between sondes and other ozone measurement techniques will need to be understood better in order to make a good estimate of the contribution to the TES bias that should actually be attributed to the ozonesondes.

[27] We compared these validation results using V002 TES data to the results of *Worden et al.* [2007] using V001 data (see Table 6). The V002 data have significant improvements to both calibration and retrieval algorithms. It should be noted that there were also differences in the approach to screening data, the coincidence criteria, the cloud criteria, and the latitude zone definitions. For example, since the coincidence criteria was not as strict by *Worden et al.* [2007], they used temperature difference as an additional criterion, assuming that large differences ($\Delta T > 5$ K over multiple levels) indicated that TES and the sonde measured different air masses. (We very rarely found $\Delta T > 5$ K over multiple levels for the present set of coincidences, and the few cases found did not appear to have poor agreement for ozone over the corresponding levels.) These changes make a direct quantitative comparison of limited value. The systematic low bias for the LT in V001 is no longer observed, while in the UT, northern hemisphere V002 results are most likely better, and tropical UT results are very similar or only very slightly better in V002.

[28] The systematic bias determined here may relate to known problems with the temperature profiles that are retrieved jointly with ozone in V002 data. Changes to the TES retrieval algorithms for V003 will use ozonesonde comparisons like these as one of the metrics for improvement. Updating the CO_2 spectroscopy is expected to result in an improvement to temperature profiles in V003 data [*Shephard et al.*, 2008b], with incremental improvements to

Table 5. Bias, Standard Deviation (σ), and the Standard Error of the Mean ($\sigma_{mean} = \sigma/\sqrt{N}$) for Different Coincidence Criteria

Coincidence Criteria	N	UT Bias ± σ, ± σ_{mean} (ppbv)	LT Bias ± σ, ± σ_{mean} (ppbv)
±9 h, 300 km	699	5.9 ± 17.8, ± 0.7	5.9 ± 12.9, ± 0.5
±3 h, 100 km	67	4.6 ± 14.4, ± 1.9	5.2 ± 11.0, ± 1.3

Table 6. TES V001 Ozone Bias and Standard Deviation From *Worden et al.* [2007]

Latitude Zone[a]	Nominal Latitude Range	N	UT Bias ± σ (ppbv)	LT Bias ± σ (ppbv)
Northern midlatitudes	25–60°N	24–27[b]	16.8 ± 18.9	−2.6 ± 6.6
Tropics	15°S–25°N	16	9.8 ± 10.3	−7.4 ± 7.0

[a]Note that these latitude zones are defined differently from those in Tables 2 and 4.
[b]The 24 is for the LT, and the 27 is for the UT.

the ozone estimates. In addition to the bias, multiple outliers were found in the northern midlatitude spring and summer, the tropics, and the northern subtopics which exhibited very high ozone values near the surface and are presumed to be erroneous. The cause of these erroneous profiles which occur with a frequency of about 1–2% (depending on the criteria used) may relate to the improper treatment of clouds or retrieval nonlinearity which is currently being quantified and will be addressed in a future publication. While correcting the problem may not be straightforward, an interim solution may be the introduction of an additional flag, similar to the emission layer flag, to identify these anomalous profiles for the average TES data user.

8. Conclusions

[29] This study used approximately 1600 TES/sonde coincidences to evaluate TES V002 nadir ozone profiles. With the present comparison method, we can rule out the role of the a priori on the TES bias and focus on systematic errors from the calibration and retrieval processes. Using this approach, a small overall positive bias was determined, with the only systematic exception (a small negative bias) in the southern subtropics between approximately 70–300 hPa (from comparisons to Reunion Island and Pretoria sonde measurements).

[30] Since TES has approximately 2 degrees of freedom for signal in the troposphere, upper troposphere and lower troposphere mean biases were determined from correlations of averages. The UT biases ranged from 2.9 ± 8.5 ppbv to 10.6 ± 15.0 ppbv considering all latitude zones. In the LT, sensitivity in the Arctic and Antarctic was very low, therefore LT values in these regions are not valid. For the remaining latitude zones, biases range from 3.7 ± 6.9 ppbv to 9.2 ± 16.3 ppbv. As a result of the size of the standard deviation or RMS relative to the bias, the exact numerical value of the bias has little meaning, but we suggest a high bias of 3–10 ppbv should be noted in scientific studies which use TES tropospheric ozone. Atmospheric variability was shown to significantly affect the matching of profile pairs; therefore, we interpret the standard deviation variability (RMS) of 7–16 ppbv, as an upper limit for the standard random variability in a single TES profile with the true value expected to be much lower. Finally, it is very important to note the linearity in TES versus sonde ozone comparisons (Figures 3 and 5), which is also impacted by atmospheric variability. Although TES ozone has biases with respect to sondes, we have confidence that the relative variations in ozone measured by TES are meaningful because of this linearity.

[31] **Acknowledgments.** Work at Harvard University was funded by grants from the National Aeronautics and Space Administration (NASA), including grant NNXO71B17G. Work performed at the Jet Propulsion Laboratory, California Institute of Technology was done under contract to NASA. We thank all those responsible for the WOUDC, SHADOZ, GMD, and IONS measurements and archives for making the ozonesonde data readily available and accessible for this work. We also thank B. Fisher, A. Eldering, R. Herman, M. Luo, and other members of the TES team who gave us comments or suggestions on this work.

References

Beer, R. (2006), TES on the Aura mission: Scientific objectives, measurements, and analysis overview, *IEEE Trans. Geosci. Remote Sens.*, *44*(5), 1102–1105, doi:10.1109/TGRS.2005.863716.

Beer, R., T. A. Glavich, and D. M. Rider (2001), Tropospheric Emission Spectrometer for the Earth Observing System's Aura satellite, *Appl. Opt.*, *40*, 2356–2367, doi:10.1364/AO.40.002356.

Bowman, K. W., T. Steck, H. M. Worden, J. Worden, S. Clough, and C. Rodgers (2002), Capturing time and vertical variability of tropospheric ozone: A study using TES nadir retrievals, *J. Geophys. Res.*, *107*(D23), 4723, doi:10.1029/2002JD002150.

Bowman, K. W., et al. (2006), Tropospheric Emission Spectrometer: Retrieval method and error analysis, *IEEE Trans. Geosci. Remote Sens.*, *44*(5), 1297–1307, doi:10.1109/TGRS.2006.871234.

Brasseur, G. P., D. A. Hauglustaine, S. Walters, P. J. Rasch, J. F. Muller, C. Granier, and X. X. Tie (1998), MOZART, a global chemical transport model for ozone and related chemical tracers: 1. Model description, *J. Geophys. Res.*, *103*, 28,265–28,289, doi:10.1029/98JD02397.

Coheur, P.-F., B. Barret, S. Turquety, D. Hurtmans, J. Hadji-Lazaro, and C. Clerbaux (2005), Retrieval and characterization of ozone vertical profiles from a thermal infrared nadir sounder, *J. Geophys. Res.*, *110*, D24303, doi:10.1029/2005JD005845.

De Backer, H., D. De Muer, and G. De Sadelaer (1998), Comparison of ozone profiles obtained with Brewer-Mast and Z-ECC sensors during simultaneous ascents, *J. Geophys. Res.*, *103*(D16), 19,641–19,648, doi:10.1029/98JD01711.

Eldering, A., S. S. Kulawik, J. R. Worden, K. W. Bowman, and G. B. Osterman (2008), Implementation of cloud retrievals for Tropospheric Emission Spectrometer atmospheric retrievals: 2. Characterization of cloud top pressure and effective optical depth retrievals, *J. Geophys. Res.*, doi:10.1029/2007JD008858, in press.

Fishman, J., and J. C. Larsen (1987), Distribution of total ozone and stratospheric ozone in the tropics: Implications for the distribution of tropospheric ozone, *J. Geophys. Res.*, *92*, 6627–6634, doi:10.1029/JD092iD06p06627.

Hudson, R. D., and A. M. Thompson (1998), Tropical tropospheric ozone from total ozone mapping spectrometer by a modified residual method, *J. Geophys. Res.*, *103*, 22,129–22,145, doi:10.1029/98JD00729.

Komhyr, W. D., R. A. Barnes, G. B. Brothers, J. A. Lathrop, and D. P. Opperman (1995), Electrochemical concentration cell ozonesonde performance evaluation during STOIC 1989, *J. Geophys. Res.*, *100*, 9231–9244, doi:10.1029/94JD02175.

Kulawik, S. S., et al. (2006a), TES atmospheric profile retrieval characterization: An orbit of simulated observations, *IEEE Trans. Geosci. Remote Sens.*, *44*(5), 1324–1332, doi:10.1109/TGRS.2006.871207.

Kulawik, S. S., J. Worden, A. Eldering, K. Bowman, M. Gunson, G. B. Osterman, L. Zhang, S. Clough, M. W. Shephard, and R. Beer (2006b), Implementation of cloud retrievals for Tropospheric Emission Spectrometer (TES) atmospheric retrievals: 1. Description and characterization of errors on trace gas retrievals, *J. Geophys. Res.*, *111*, D24204, doi:10.1029/2005JD006733.

Liu, X., K. Chance, C. E. Sioris, R. J. D. Spurr, T. P. Kurosu, R. V. Martin, and M. J. Newchurch (2005), Ozone profile and tropospheric ozone retrievals from the Global Ozone Monitoring Experiment: Algorithm description and validation, *J. Geophys. Res.*, *110*, D20307, doi:10.1029/2005JD006240.

Liu, X., et al. (2006), First directly retrieved global distribution of tropospheric column ozone from GOME: Comparison to the GEOS-Chem model, *J. Geophys. Res.*, *111*, D02308, doi:10.1029/2005JD006564.

Logan, J. A. (1999), An analysis of ozonesonde data for the troposphere: Recommendatinos for testing 3-D models and development of a gridded climatology for tropospheric ozone, *J. Geophys. Res.*, *104*(D13), 16,115–16,149, doi:10.1029/1998JD100096.

Osterman, G., et al. (2006), *Tropospheric Emission Spectrometer TES L2 Data User's Guide, Version 2.00, 1 June 2006*, Jet Propul. Lab., Calif. Inst. of Technol., Pasadena, Calif.

Park, M., W. J. Randel, D. E. Kinnison, R. R. Garcia, and W. Choi (2004), Seasonal variations of methane, water vapor, ozone, and nitrogen dioxide near the tropopause: Satellite observations and model simulations, *J. Geophys. Res.*, *109*, D03302, doi:10.1029/2003JD003706.

Richards, N., G. B. Osterman, E. V. Browell, J. Hair, M. A. Avery, and Q. B. Li (2008), Validation of Tropospheric Emission Spectrometer (TES) ozone profiles with aircraft observations during INTEX-B, *J. Geophys. Res.*, doi:10.1029/2007JD008815, in press.

Rodgers, C. D. (2000), Inverse Methods for Atmospheric Sounding: Theory and Practice, World Sci., London.

Rodgers, C. D., and B. J. Connor (2003), Intercomparison of remote sounding instruments, *J. Geophys. Res.*, *108*(D3), 4116, doi:10.1029/2002JD002299.

Shephard, M. W., et al. (2008a), Comparison of Tropospheric Emission Spectrometer (TES) nadir water vapor retrievals with in situ measurements, *J. Geophys. Res.*, doi:10.1029/2007JD008822, in press.

Shephard, M. W., et al. (2008b), Tropospheric Emission Spectrometer nadir spectral radiance comparisons, *J. Geophys. Res.*, doi:10.1029/2007JD008856, in press.

Smit, H. G. J., et al. (2007), Assessment of the performance of ECC-ozonesondes under quasi-flight conditions in the environmental simulation chamber: Insights from the Juelich Ozone Sonde Intercomparison Experiment (JOSIE), *J. Geophys. Res.*, *112*, D19306, doi:10.1029/2006JD007308.

Stratospheric Processes and their Role in Climate, International Ozone Commision, and Global Atmosphere Watch (1998), Assessment of trends in the vertical distribution of ozone: Report #1, edited by N. Harris, R. Hudson, and C. Phillips, *World Meteorol. Organ. Ozone Res. and Monit. Proj. Rep. 43*, Geneva, Switzerland. (Available at http://www.atmosp.physics.utoronto.ca/SPARC/)

Thompson, A. M., et al. (2003a), Southern Hemisphere Additional Ozonesondes (SHADOZ) 1998–2000 tropical ozone climatology: 1. Comparison with Total Ozone Mapping Spectrometer (TOMS) and ground-based measurements, *J. Geophys. Res.*, *108*(D2), 8238, doi:10.1029/2001JD000967.

Thompson, A. M., et al. (2003b), Southern Hemisphere Additional Ozonesondes (SHADOZ) 1998–2000 tropical ozone climatology: 2. Tropospheric variability and the zonal wave-one, *J. Geophys. Res.*, *108*(D2), 8241, doi:10.1029/2002JD002241.

Thompson, A. M., J. C. Witte, H. G. J. Smit, S. J. Oltmans, B. J. Johnson, W. J. H. V. Kirchhoff, and F. J. Schmidlin (2007a), Southern Hemisphere Additional Ozonesondes (SHADOZ) 1998–2004 tropical ozone climatology: 3. Instrumentation, station variability, evaluation with simulated flight profiles, *J. Geophys. Res.*, *112*, D03304, doi:10.1029/2005JD007042.

Thompson, A. M. (2007b), Intercontinental Chemical Transport Experiment Ozonesonde Network Study (IONS) 2004: 2. Tropospheric ozone budgets and variability over northeastern North America, *J. Geophys. Res.*, *112*, D12S13, doi:10.1029/2006JD007670.

Thompson, A. M., et al. (2007c), Intercontinental Chemical Transport Experiment Ozonesonde Network Study (IONS) 2004: 1. Summertime upper troposphere/lower stratosphere ozone over northeastern North America, *J. Geophys. Res.*, *112*, D12S12, doi:10.1029/2006JD007441.

Turquety, S., J. Hadji-Lazaro, and C. Clerbaux (2002), First satellite ozone distributions retrieved from nadir high-resolution infrared spectra, *Geophys. Res. Lett.*, *29*(24), 2198, doi:10.1029/2002GL016431.

Valks, P. J. M., R. B. A. Koelemeijer, M. van Weele, P. van Velthoven, J. P. F. Fortuin, and H. Kelder (2003), Variability in tropical tropospheric ozone: Analysis with Global Ozone Monitoring Experiment observations and a global model, *J. Geophys. Res.*, *108*(D11), 4328, doi:10.1029/2002JD002894.

Worden, H. M., et al. (2007), Comparisons of Tropospheric Emission Spectrometer (TES) ozone profiles to ozonesondes: Methods and initial results, *J. Geophys. Res.*, *112*, D03309, doi:10.1029/2006JD007258.

Worden, J. S., S. S. Kulawik, M. Shepard, S. Clough, H. Worden, K. Bowman, and A. Goldman (2004), Predicted errors of Tropospheric Emission Spectrometer nadir retrievals from spectral window selection, *J. Geophys. Res.*, *109*, D09308, doi:10.1029/2004JD004522.

Ziemke, J. R., S. Chandra, and P. K. Bhartia (1998), Two new methods for deriving tropospheric column ozone from TOMS measurements: Assimilated UARS MLS/HALOE and convective-cloud differential techniques, *J. Geophys. Res.*, *103*, 22,115–22,127, doi:10.1029/98JD01567.

Ziemke, J. R., S. Chandra, and P. K. Bhartia (2005), A 25-year data record of atmospheric ozone in the Pacific from Total Ozone Mapping Spectrometer (TOMS) cloud slicing: Implications for ozone trends in the stratosphere and troposphere, *J. Geophys. Res.*, *110*, D15105, doi:10.1029/2004JD005687.

Ziemke, J. R., S. Chandra, B. N. Duncan, L. Froidevaux, P. K. Bhartia, P. F. Levelt, and J. W. Waters (2006), Tropospheric ozone determined from Aura OMI and MLS: Evaluation of measurements and comparison with the Global Modeling Initiative's Chemical Transport Model, *J. Geophys. Res.*, *111*, D19303, doi:10.1029/2006JD007089.

S. Austin, Medgar Evers College, City University of New York, 1650 Bedford Avenue, Brooklyn, NY 11225, USA. (saustin@mec.cuny.edu)

K. W. Bowman and G. B. Osterman, Jet Propulsion Laboratory, 4800 Oak Grove Drive, Mail Stop 183-601, Pasadena, CA 91109, USA. (kevin.bowman@jpl.nasa.gov; gregory.b.osterman@jpl.nasa.gov)

H. Claude, Deutscher Wetterdienst Meteorologisches Observatorium Hohenpeissenberg, Albin-Schwaiger-Weg 10, D-82383 Hohenpeissenberg, Germany. (hans.claude@dwd.de)

M. K. Dubey, Los Alamos National Laboratory, P.O. Box 1663, Los Alamos, NM 87545, USA. (dubey@lanl.gov)

W. K. Hocking, Department of Physics and Astronomy, University of Western Ontario, 1151 Richmond Street North, London, ON, Canada N6A 3K7. (whocking@uwo.ca)

B. J. Johnson and S. J. Oltmans, NOAA Earth System Research Laboratory, 325 Broadway Street, Boulder, CO 80305-3328, USA. (bryan.johnson@noaa.gov; samuel.j.oltmans@noaa.gov)

E. Joseph, Physics and Astronomy Department, Howard University, 2400 Sixth Street NW, Washington, DC 20059, USA. (ejoseph@howard.edu)

J. A. Logan, I. A. Megretskaia, and R. Nassar, Harvard University, Pierce Hall, 29 Oxford Street, Cambridge, MA 02138, USA. (jal@io.harvard.edu; iam@io.harvard.edu; ray@io.as.harvard.edu)

J. Merrill, Graduate School of Oceanography, University of Rhode Island, 215 South Ferry Road, Narragansett, RI 02882, USA. (jmerrill@gso.uri.edu)

G. A. Morris, Department of Physics and Astronomy, Valparaiso University, 1610 Campus Drive East, Valparaiso, IN 46383, USA. (gary.morris@valpo.edu)

M. Newchurch, National Space Science and Technology Center, Atmospheric Science Department, University of Alabama in Huntsville, 320 Sparkman Drive, Huntsville, AL 35805, USA. (mike@nsstc.uah.edu)

F. Posny, Laboratoire de l'Atmosphère et des Cyclones, UMR 8105, CNRS/Université de la Réunion, 15 avenue Rene Cassin, F-97715, Saint-Denis Messag cedex 9, La Réunion, France. (francoise.posny@univ-reunion.fr)

F. J. Schmidlin, Laboratory for Hydrospheric Processes, Observational Science Branch, NASA/Wallops Flight Facility, Wallops Island, VA 23337, USA. (fjs@osb1.wff.nasa.gov)

D. W. Tarasick, Experimental Studies, Air Quality Research Division, Environment Canada, 4905 Dufferin Street, Downsview, ON, Canada M3H 5T4. (david.tarasick@ec.gc.ca)

A. M. Thompson, Department of Meteorology, Pennsylvania State University, 503 Walker Building, University Park, PA 16802-5012, USA. (anne@met.psu.edu)

H. Vömel, Cooperative Institute for Research in Environmental Studies, University of Colorado, Campus Box 216, Boulder, CO 80309-0216, USA. (holger.voemel@colorado.edu)

D. N. Whiteman, Mesoscale Atmospheric Processes Branch, Goddard Space Flight Center, NASA, Code 613.1 Building 33, Room D404, Greenbelt, MD 20771, USA. (david.n.whiteman@nasa.gov)

J. C. Witte, Atmospheric Chemistry and Dynamics Branch, Goddard Space Flight Center, NASA/Science Systems and Applications, Inc., Code 613.3, Greenbelt, MD 20771, USA. (witte@gavial.gsfc.nasa.gov)

H. M. Worden, Atmospheric Chemistry Division, National Center for Atmospheric Research, P.O. Box 3000, Boulder, CO 80305-3000, USA. (hmw@ucar.edu)